Available online at website: https://journal.bcrec.id/index.php/bcrec

Bulletin of Chemical Reaction Engineering & Catalysis, 19 (4) 2024, 692-709

Research Article

Energy-efficient Carbon-doped TiO_2 for Visible Light Degradation of Methyl Orange: Preparation, Performance, and Mechanism

Xinying Han[1], Yubei Guo[1], Chien Yong Goh[2], Cheng Loong Ngan[1,3], Jian Ping Tan[1,3], Peng Chee Tan[1,3], Sin Yuan Lai[1,3,*]

[1]School of Energy and Chemical Engineering, Xiamen University Malaysia, Jalan Sunsuria, Bandar Sunsuria, 43900 Sepang, Selangor, Malaysia.
[2]Department of Mathematics, Xiamen University Malaysia, Jalan Sunsuria, Bandar Sunsuria, 43900 Sepang, Selangor, Malaysia
[3]College of Chemistry and Chemical Engineering, Xiamen University, 361005 Xiamen, China.

Received: 27th October 2024; Revised: 5th December 2024; Accepted: 6th December 2024
Available online: 7th December 2024; Published regularly: December 2024

Abstract

Water pollution caused by textile dyes has become a serious issue, making the treatment of sewage urgent. Carbon-doped TiO_2 (C-doped TiO_2), using alkanes and polyols as carbon sources, has been found to be light-responsive in degrading dyes. However, there is a lack of studies on the interfacial interaction between carboxylic acids and TiO_2. Therefore, citric acid, a triprotic, hexadentate carboxylic acid, was used to dope TiO_2 through solvothermal-calcination. The effects of carbon content and calcination temperature on the photodegradation performance of C-doped TiO_2 were investigated. The band gap energy of C-doped TiO_2 was found to be narrower (2.67 eV) than that of undoped TiO_2 (2.88 eV). After carbon doping, the absorption band extended from the UV to the visible regions, lowering the energy required for electron excitation. The functional groups present on C-doped TiO_2 assisted in the adsorption of methyl orange (MO), assisting in photodegradation. Only the anatase phase of TiO_2 was observed at calcination temperatures between 250 and 400 °C. Photoluminescence analysis revealed that a lower carbon content and slightly higher calcination temperature resulted in better interfacial charge separation and transfer efficiency. The 10 wt% C-doped TiO_2 calcined at 300 °C demonstrated the best MO photodegradation efficiency of 62.1% under visible light illumination.

Keywords: energy efficient; carbon-doped TiO2; wastewater treatment; green synthesis; photodegradation

How to Cite: Han, X., Guo, Y., Goh, C.Y., Ngan, C.L., Tan, J.P., Tan, P.C., Lai, S.Y. (2024). Energy-efficient Carbon-doped TiO2 for Visible Light Degradation of Methyl Orange: Preparation, Performance, and Mechanism. *Bulletin of Chemical Reaction Engineering & Catalysis*, 19 (4), 692-709 (doi: 10.9767/bcrec.20236)

Permalink/DOI: https://doi.org/10.9767/bcrec.20236

1. Introduction

Nowadays, the shortage of water resources has seriously affected human's normal survival. Water contamination is one of the main causes of water shortage. And among all the water pollutants, the organic molecule is the particularly troubling because it is hard to decolorize and has long-term accumulation which causes food chain contamination and harm to human beings [1,2]. With the rapid development of textile industry, excessive organic dyestuffs discharge into the aquatic environment. There are about 10,000 different synthetic dyes on the market, and worldwide annual production of these dyes exceeds 700,000 tons. Nearly 200,000 tons of synthetic dyes are lost to the environment due to inefficient dyeing processes in the textile industry [3]. Therefore, organic dyes have become a typical industry organic pollutant. Methyl orange is one of the organic dyes usually uses in the textile industry. Because methyl orange is toxic, the emission of methyl orange will directly affect aquatic environment. Developing advanced materials and methods to decontaminate water has attracted many researchers' interests.

* Corresponding Author.
Email: sinyuan.lai@xmu.edu.my;
sinyuan12@gmail.com (Sin Yuan Lai)

Currently, there are three common methods used for wastewater treatment, which are absorption, membranes technologies, and photocatalytic degradation. For absorption method, it could not degrade the pollutants and would generate a large amount of hazardous solid and liquid wastes [1]. Membrane technologies is not an economic method because of its expensive raw material and high fabrication cost [4]. Photocatalytic degradation relies on sunlight energy without mechanical energy consumption and will not produce secondary pollution, is considered as a clean, economical, environmentally friendly technology [2]. Another important advantage of photocatalysis is that it could remove the low concentration of pollutants which are not discarded by coagulation, flocculation, and filtration. The photo-oxidation works even at very low contaminant concentrations (even at ppt) because the contaminant is attracted strongly to the surface of the catalyst [5]. Hence, photocatalysts provide a great potential in the wastewater treatment field.

Semiconductors are widely used in the photocatalytic industry because of their ability to absorb energy and produce electron-hole pairs to participate in redox reactions [6–8]. Titanium dioxide (TiO_2) as a common semiconductor photocatalyst because of its chemical stability, low cost, low-toxicity and high efficiency in the removal of pollutants in water and air usually uses in water splitting to produce hydrogen, degradation of organic pollutants in atmosphere or aquatic environment, and photoelectrochemical solar cell [1,2,9]. However, TiO_2 has a wide bandgap (3.0 eV-3.2 eV), which limiting its charge separation effective under the ultraviolet light, therefore, TiO_2 only uses 5% of the solar spectrum to yield the photocatalytic reactions involved in water purification [9,10]. Another drawback of TiO_2 is its high recombination rate of its photogenerated electron and holes. In recent years, researchers have found that doping is an efficient method to improve the photoactivity of TiO_2 under visible light and reduce the recombination of the electrons and holes. Owing to the precursor of carbon doping is cheap and easy to get, so carbon element becomes a popular nonmetal doping element for TiO_2 doping research [11].

Past studies have focused on the alkane, disaccharide, alcohol, and polymer such as hexane [12], glucose [13,14], ethylene glycol [15] and polyol [16], as the doping agents to narrow the wide band gap of TiO_2, and resulting in lower the calcination temperature (energy efficiency). Doping with the aforementioned carbon materials, the absorption band can be extended to a longer wavelength (visible light responsiveness) correspondingly. Additionally, these carbon materials are primarily composed of hydroxyl groups (–OH), which can aid in pollutant adsorption on the catalyst surface, meanwhile, the –OH groups facilitate electron separation and transfer, leading to the formation of superoxide ($\bullet O_2^-$) and hydroperoxyl ($\bullet OOH$) radicals, which subsequently degrades the adsorbed pollutants. High temperature sintering, chemical vapor deposition and solution-phase strategies are three important synthesis methods for C-doped TiO_2, but they are high-temperature treatment, expensive, toxic, or unstable precursor, and tedious procedure [11]. Therefore, developing a green, facile, and energy efficient approach for synthesis of C-doped TiO_2 with high visible photocatalytic activity is significant. Up to date, lack of findings on utilizing the carboxylic acid-based compounds to modify the TiO_2 through green and facile preparation routes. To date, only one literature [17] reported that a bidentate carboxylate ligand, i.e. acetic acid, doped onto TiO_2, demonstrating 100% methyl orange and 96.4% phenol photodegradation after 75-min light illumination. The good photocatalytic performance is owing to the strong interaction between the interstitial lattice of carbon dopant and TiO_2, in conjuncture of elevation of the valence band in narrowing the band gap, thus inducing band tail states that enhance the visible light absorption.

In this study, bio-based hexadentate carboxylic acid, i.e. citric acid, is used to dope with TiO_2 through solvothermal-calcination strategies. The research aims to produce an energy-efficient C-doped TiO_2, to investigate the interstitial of carbon within TiO_2 framework, Ti-O-C phase shifting, anatase TiO_2 phase crystallinity, the band gap (<3.2 eV), and charge separation and transfer. The research also aims to evaluate the C-doped TiO_2 photocatalytic efficiency using a complex, azo anionic dye, methyl orange (MO), under visible-light (100 W) illumination for 2 h.

2. Materials and Method

2.1 Materials

Titanium n-butoxide ($Ti(C_4H_9O)_4$), TBT, 0.998g/mL, Sigma-Aldrich), citric acid ($C_6H_8O_7$, Sigma-Aldrich), methyl orange ($C_{14}H_{14}N_3NaO_3S$, MO), hydrogen chloride (HCl, Merk), sodium hydroxide (NaOH, Sigma-Aldrich), acetic acid (CH_3COOH, Merk), ethanol (CH_3CH_2OH, Merk), phosphoric acid (H_3PO_4, Merk). All chemicals used in this study are of analytical grade and were used without further purification. Distilled water was used in all experiments.

2.2 Synthesis of Carbon-doped TiO_2

The carbon-doped TiO_2 (C-doped TiO_2) was prepared by solvothermal-calcination method as shown in Figure 2. In the solvothermal synthesis process, TBT was used as precursor and citric acid

was used as carbon source for C-doped TiO_2. First, three solutions were prepared – Solution (1): 1 mL CH_3COOH was dissolved in 10 mL distilled water and stirred for 5 min; Solution (2): 6 mL TBT was dissolved in 20 mL 95% ethanol and stir for 5 min; Solution (3): The citric acid was mixed with 20 mL 95% ethanol. After that, TBT solution was added dropwise into the CH_3COOH solution under 400 rpm stirring speed to form TiO_2 sols (refer to Figure 1). The citric acid was added dropwise into the mixture containing TBT and acetic acid.

The citric acid concentrations were varied at 10 wt%, 30 wt% and 50 wt%. The mixture solution was sonicated for 10 min. After under 400 rpm stirring for 1 h, the colloidal solution was transferred to 100 mL Teflon-lined autoclave and solvothermally treated at 180 °C for 10 h. The sample obtained were filtered, washed with water three times, and dried at 120 °C in an oven at atmospheric pressure overnight. Subsequently, the undoped TiO_2 and C-doped TiO_2 were calcined at 250, 300, 400 °C in a muffle furnace for 3 h with ramping rate of 5 °C /min. Then the as-synthesized samples are labelled as *x*wt%C-TiO_2-*y*, where the *x* is the carbon loading and *y* is the calcination temperature. Please refer to Table 1 for all of the denotations.

Table 1. The denotation of C-doped TiO_2, *x*wt%C-TiO_{2-y}, at their respective carbon amount and calcination temperature.

Photocatalyst	Carbon amount (wt%)	Calcination Temperature (°C)
TiO_2-250	-	250
10wt%C-TiO_2-250	10	250
30wt%C-TiO_2-250	30	250
50wt%C-TiO_2-250	50	250
TiO_2-300	-	300
10wt%C-TiO_2-300	10	300
30wt%C-TiO_2-300	30	300
50wt%C-TiO_2-300	50	300
TiO_2-400	-	400
10wt%C-TiO_2-400	10	400
30wt%C-TiO_2-400	30	400
50wt%C-TiO_2-400	50	400

2.3 Catalyst Characterizations

2.3.1 X-ray diffraction (XRD)

The identification of crystalline phases in C-doped TiO_2 is performed using X-ray diffraction (XRD) analysis, utilizing Cu-K_α radiation. The XRD analysis of the prepared photocatalysts was

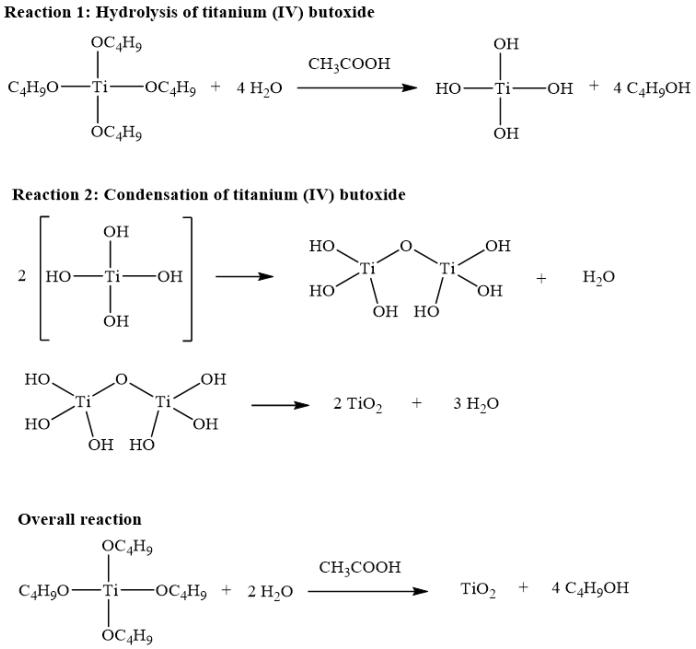

Figure 1. Hydrolysis and condensation reaction of titanium(IV) butoxide to form TiO_2 sols.

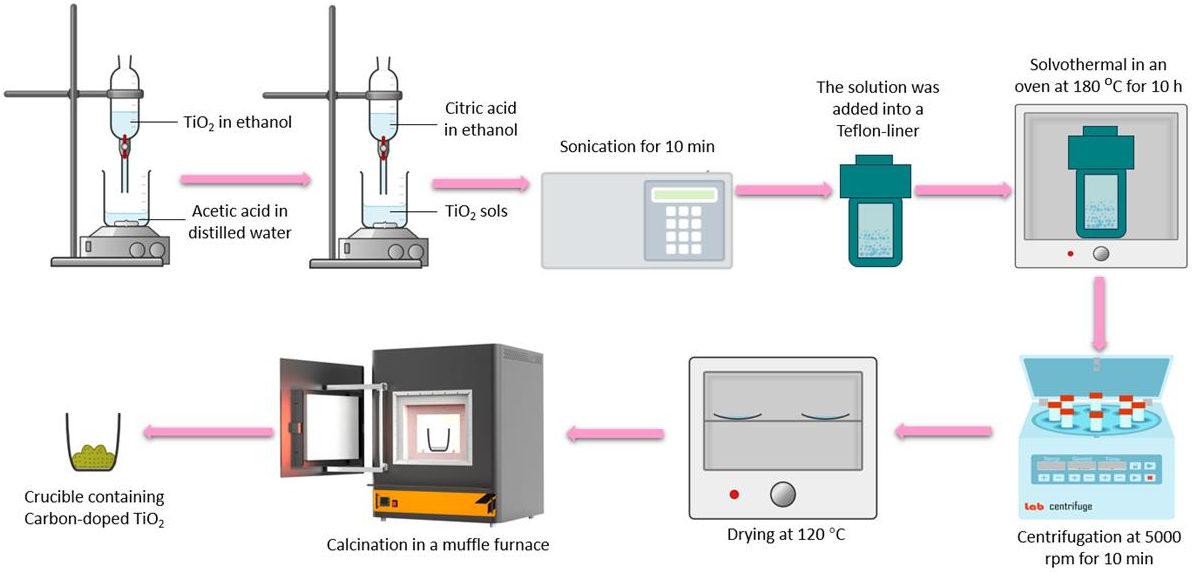

Figure 2. Schematic procedure of producing C-doped TiO_2 using solvothermal and calcination approaches.

conducted at room temperature using Cu-K_α radiation with a wavelength of 0.15406 nm. A graphite monochromator was employed, operated at 40 kV and 30 mA. The diffraction patterns were recorded within the angular range of 10-80°, with a step width of 0.05° s^{-1}. By examining the resulting diffraction patterns, valuable information regarding the crystalline phases present in the C-doped TiO_2 can be determined. This XRD analysis enables the characterization and identification of the crystal structures within the C-doped TiO_2 material, aiding in the understanding of its composition and properties.

The Debye-Scherrer equation presented in Equation (1) was used to calculate the crystallite size or grain size of the as-synthesized C-doped TiO_2.

$$D = \frac{k\lambda}{\beta \cos\theta} \quad (1)$$

Where, D is the crystallite size or grain size (nm) of plane (101) for anatase TiO_2, K is the shape factor (Scherrer constant), 0.94, for spherical crystallite; λ is the X-ray wavelength, Cu-K_α = 1.5406 Å (0.15406 nm); β is the full width at half-maximum height (FWHM) of the peak (measured in radians); and θ is the Bragg's angle in degrees, half of 2θ.

2.3.2 Diffuse reflectance ultraviolet-visible (DR UV-vis) spectroscopy

The absorption range of the pure TiO_2 and the modified C-doped TiO_2 are determined by the UV-vis diffusive reflectance (DR UV-vis, brand: Shimadzu) in the wavelength of 200–800 nm, equipped with an integrating sphere assembly, using $BaSO_4$ as the reflectance sample. A wavelength (x-axis) vs absorbance (y-axis) curve is plotted and Tauc Plot is plotted out using these equations, $E = 1240 / \lambda$, on the x-axis and $(ahv)^2$ on the y-axis. The n = 1/2 is used due to its direct allowed transition.

2.3.3 Fourier-transform infrared (FTIR) spectroscopy

Photocatalysts were preheated at 60 °C for few hours as a precaution step to ensure that the dried samples mixed well with KBr powder and get a compact and transparent disk for infrared analysis. The sample to KBr ratio was 1:100. The FTIR spectra were collected on a Perkin Elmer Spectrum One spectrometer with 15 scans and resolution of 4 cm^{-1}, in the range of 4000 – 400 cm^{-1}. The KBr pellet technique is used to examine the bonding characteristics of functional groups in undoped TiO_2 and C-doped TiO_2 photocatalysts at a series of wt% and a range of calcination temperatures.

2.3.4 Photoluminescence (PL) spectroscopy

The photoluminescence (PL) emission spectra of the synthesized catalysts were measured using fluorescence with Xe lamp as excitation source. The recombination rate of electron-hole and charge transfer mechanism were disclosed by the photoluminescence emission at the range of 500 – 550 nm. PL emission spectra were measured on a luminescence spectrometer (Cary Eclips) at room temperature under the excitation light at 265 nm.

2.4 Photocatalytic Activity Evaluation

The photocatalytic activity of synthesized catalysts was investigated by evaluating the decomposition of the methyl orange (MO) (Figure 3). The effect of dopant concentration and calcination temperature of 0.1 g photocatalyst was investigated by the degradation of 500 mL of 25 ppm MO. The pH of the solution was adjusted to acidic environment, ~3.3, using H_3PO_4 solution. The MO in acidic aqueous solution was stirred for 30 min using a magnetic stirrer under the dark condition (light-off) to reach the adsorption-desorption equilibrium. After 30 min, the degradation of MO was performed at room temperature for 2 h using a photocatalytic reactor

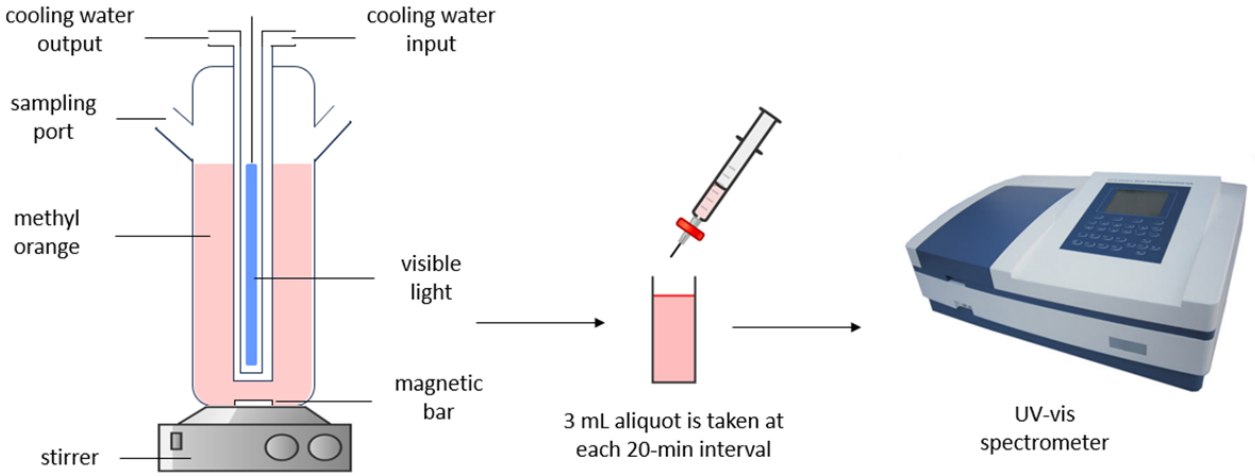

Figure 3. Schematic flow of photocatalytic activity of C-doped TiO_2 in degrading methyl orange pollutan.

under irradiation of a Xe lamp source (100 W). The 3 mL suspension was drawn into small centrifuge tubes for separation and analysis at every 20-min interval for 2 h. Please refer to the procedure flow in Figure 3.

The concentration of MO was monitored by recording the maximum absorbance of MO at 465 nm with a UV–vis spectrophotometer. The degradation efficiency was determined using Equation (2):

$$Degradation\ (\%) = \frac{(C_0 - C_t)}{C_0} \times 100\% \qquad (2)$$

where, C_0 is the MO dye concentration before degradation and C_t is the MO dye concentration after certain time t.

3. Results and Discussions

3.1 FTIR Characterization

Figure 4(a) depicts several functional groups of citiric acid, including –COOH (1780-1710 cm^{-1}), OH stretching (3550-3200 cm^{-1}), C–O (1205-1124 cm^{-1}), C=O (1780-1630 cm^{-1}), and C–H bending (1465-1380 cm^{-1}). Figure 4(b) displays the undoped TiO_2 peaks at 3454.21 cm^{-1}, 1631.78 cm^{-1} and 690.52 cm^{-1}, which are attributed to the -OH stretching, –OH bending and Ti–O stretching bands, respectively.

3.1.1 Effect of carbon amount

As depicted in Figure 5, the broad peak around 3300 – 3400 cm^{-1}, which are originating from the stretching vibration mode of surface absorbed water and hydroxyl group. The broad peak around 3300 – 3400 cm^{-1}, which are

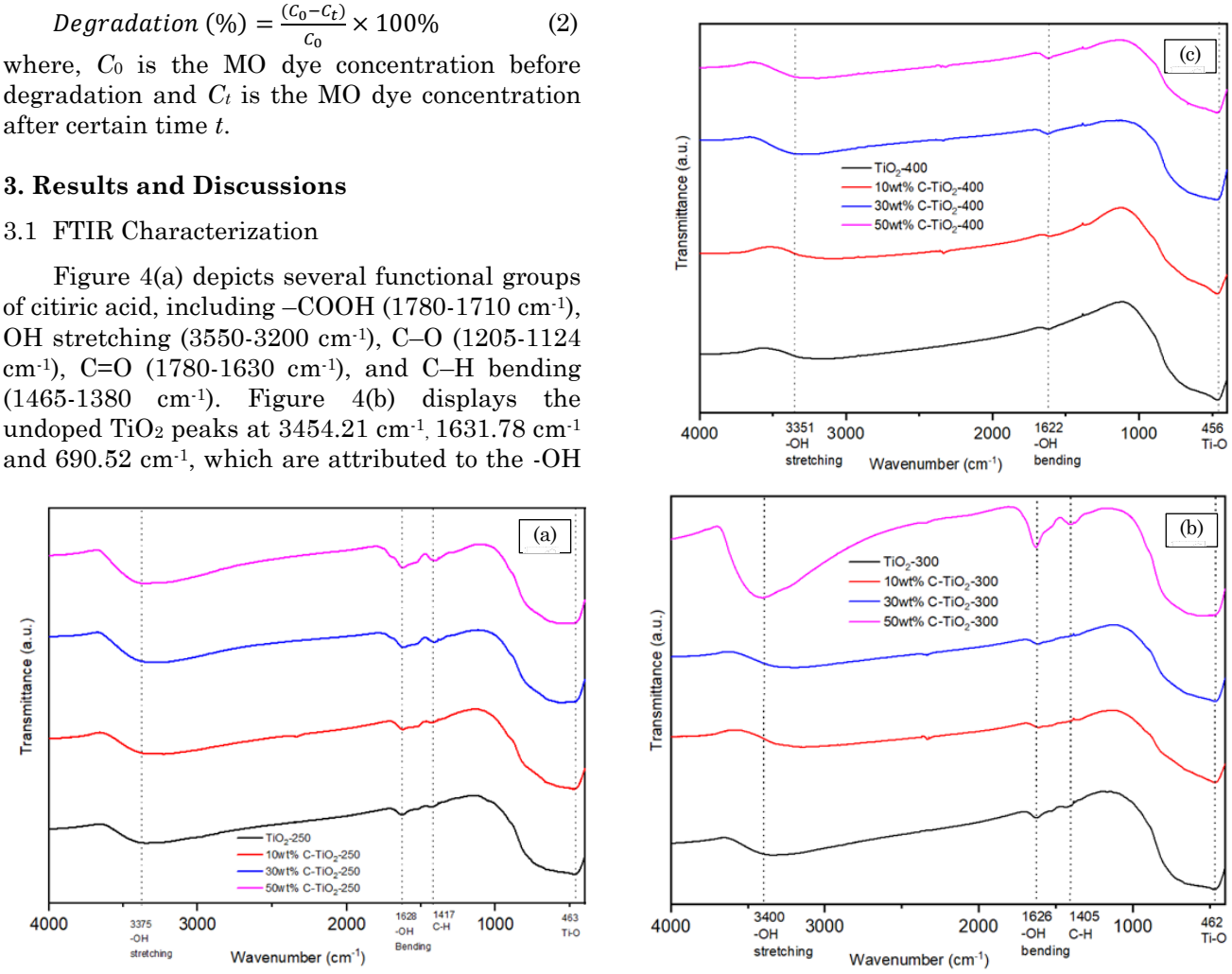

Figure 5. FTIR spectra of TiO_2 and C-doped TiO_2 with varied carbon amount of 10, 30 and 50 wt% at (a) 250 °C, (b) 300 °C, and (c) 400 °C.

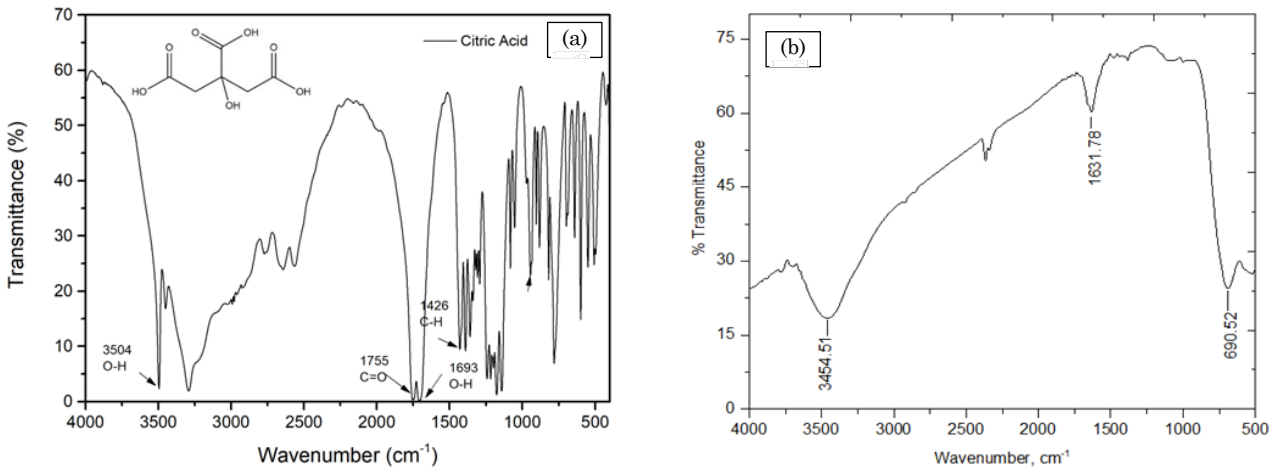

Figure 4. FTIR spectra of (a) Citric acid, (b) TiO_2

originating from the stretching vibration mode of surface absorbed water and hydroxyl group. The narrow peak around 1625 – 1630 cm^{-1}, which is attributed to the bending vibration mode of O–H bond from hydroxyls and coordinated water as well as form the Ti-OH group [18]. The absorbed water and hydroxyl groups present usually on the surface of the transition metal; oxides and are considered as an important factor of the surface properties of the transition metal oxide. The bending vibration absorption peak of C–H appears near the 1400 cm^{-1}. The spectra shows that the C-doped TiO_2 had a common peak around 1400 cm^{-1}, which identify the existence of the carbon-related substrate on the surface. The 50 wt% carbon doping content always has the sharpest peak at 1400 cm^{-1} at every calcination temperature means it has most carbonaceous materials on the surface. Can see that when the calcination is 250 °C, this is peak is obvious to see, when the calcination temperature increases, the peak is weaker suggests that the carbonaceous materials is eliminated during calcination. Under 400 °C of calcination, there are no peaks in the 1400 cm^{-1}, which means that carbonaceous materials have decomposed at 400 °C. The spectra shows that the undoped TiO_2-250 also has peak around 1400 cm^{-1}, the carbon substrate may come from the titanium(IV) butoxide and ethanol used in the synthesis process. The spectra of undoped TiO_2 and C-doped TiO_2 all show a characteristic band in the 400 cm^{-1} to 1000 cm^{-1} associated to TiO_2 materials, because the IR bands in the region from 400 cm^{-1} to 1000 cm^{1} are highly sensitive to the Ti-O-Ti band. The peak around 460 cm^{-1} is attributed to the stretching vibration of Ti–O of TiO_2 [13].

3.1.2 Effect of calcination temperature

Comparing the intensity peak around 3200 cm^{-1} to 3400 cm^{-1} in Figure 6, FTIR spectra of (a), (b), (c) and (d), can find that the peak intensity decreases when the temperature increases, which may be cause by the loss of absorbed water in the surface of catalysts during calcination. Comparing the peak intensity around the 1400 cm^{-1} which are related to the carbonaceous species, it is observed that the peak intensity decreases when the temperatures are increasing. The peak intensities of 10 wt% and 30 wt% doped TiO_2 at the 300 and 400 °C are very weak, indicating the carbonaceous materials are almost completely decomposed. The 50 wt% doped TiO_2 displays absorption peaks at the 250 and 300 °C, but the peak does not appear

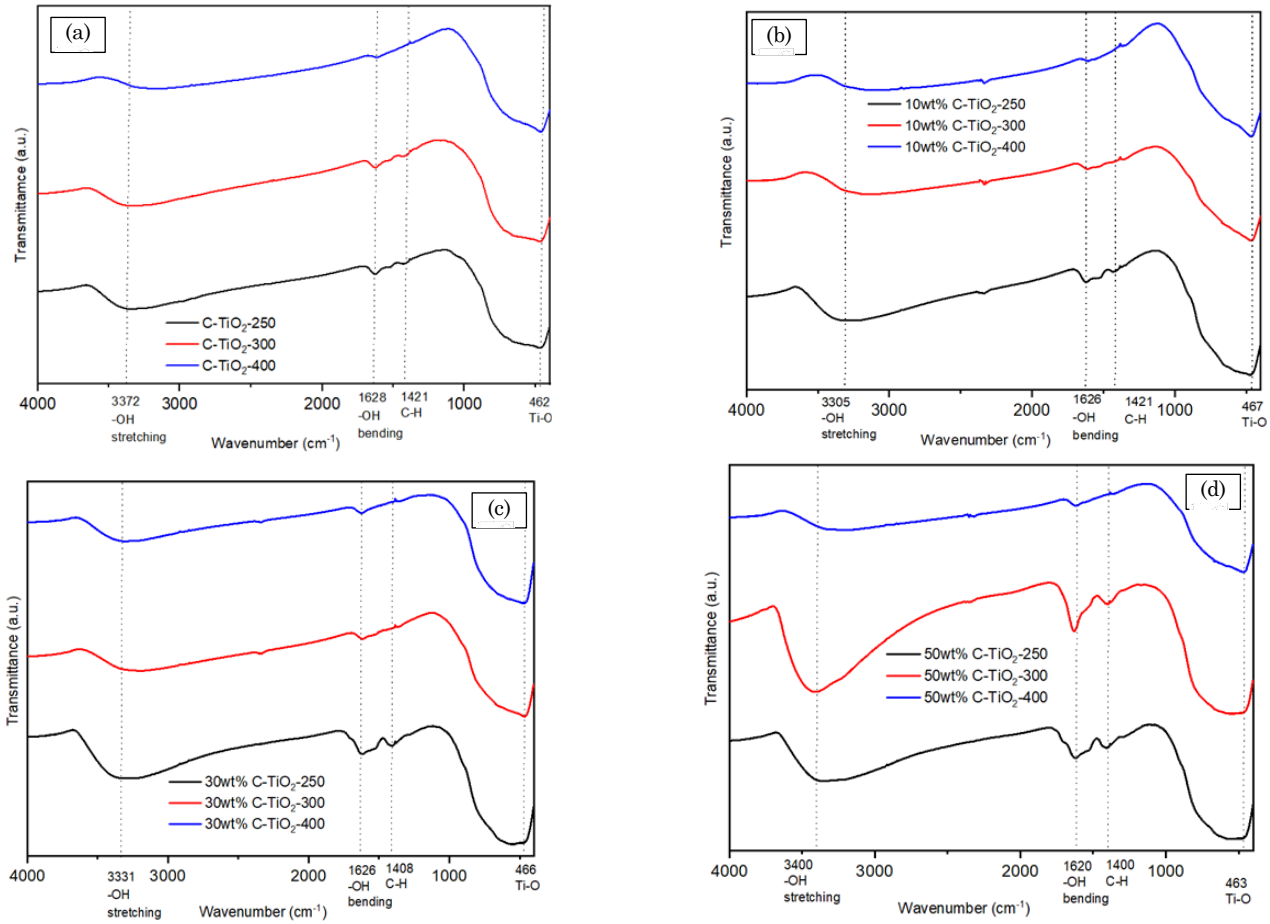

Figure 6. FTIR spectra of (a) TiO_2, (b) C-doped TiO_2-10 wt%, (c) C-doped TiO_2-30 wt%, (d) C-doped TiO_2-50 wt% at 200, 300, and 400 °C.

in the 400 °C, which indicated that the carbonaceous species on the surface completely decomposed at 400 °C.

3.2 DR UV-Vis Characterization

3.2.1 The effect of carbon amount towards band gap energy

All of the C-doped TiO_2 samples exhibit an extended absorption edge (> 400 nm) compared to undoped TiO_2 (~ 400 nm). The colour of undoped TiO_2, 10wt%C-TiO_2, 30wt%C-TiO_2 and 50wt%C-TiO_2 has changed from white to yellow and brown with an increasing of carbon content, evidencing an extended absorption light as well. It also suggests that the carbon is incorporated into TiO_2 lattice attributed by introducing a series of localized occupied states into the band gap of TiO_2 lattice [18]. The 10wt%C-TiO_2-400 reflecting the light yellow has the similar reflectance spectra as the undoped TiO_2-400, which may be caused by the carbon doped into the TiO_2 lattice was burnt out at a higher calcination temperature. Based on another literature, Kavitha *et al*. [13] used glucose to synthesize the C-TiO_2 (0.04 wt%), C-TiO_2 (0.06 wt%), C-TiO_2 (0.08 wt%) and C-TiO_2 (0.1 wt%), respectively, and the bandgap energy of these catalysts decreased from 2.95 eV to 2.83 eV with the increasing of the carbon dopant content. What's more, the 0.04 wt% C-doped TiO_2 with the

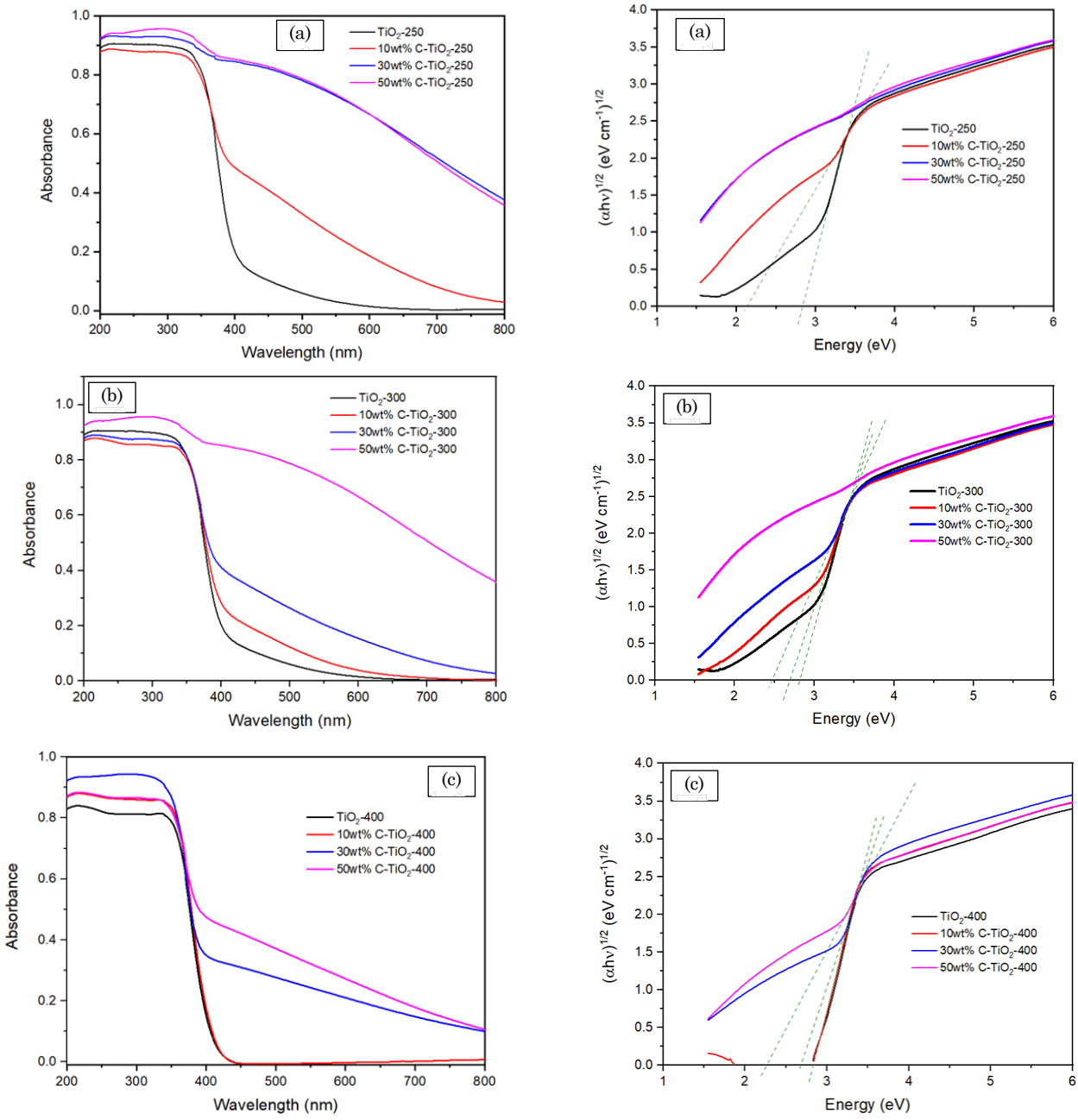

Figure 7. The diffuse reflectance spectra and the Kubelka-Munk plots for undoped TiO_2 and C-doped TiO_2 with varied carbon amount of 10 wt%, 30 wt%, and 50 wt% at (a) 250 °C, (b) 300 °C, and (c) 400 °C.

bandgap energy of 2.95 eV has the best performance on the photodegradation which may indicate that there exists an optimum bandgap energy having the lower excitation energy and the less photogenerated electrons jumping back to valence band [13].

3.2.2 The effect of calcination temperature towards the band gap energy

Figure 8 shows all of the undoped TiO_2 have the similar reflectance spectra, Kubelka-Munk Plots and bandgap energy. Figures 8(b) and (c) illustrates that the absorption bands of C-doped TiO_2 produced under a lower calcined temperature (250 and 300 °C) have an extended edged compare to a higher calcined temperature (400 °C). This can be explained that the absorption band region is extended with decreasing calcined temperature given the same carbon content in the photocatalyst. In addition, it is also observed that the band gap energy decreases when calcination temperature decreases given the same carbon content. Based on a literature, Park *et al*. [19] has examined the absorption range of C-doped TiO_2 calcined at 250, 300, and 400 °C, demonstrating that the C-doped TiO_2 calcined at the 250 °C has the largest absorption range with a bandgap energy of 2.8 eV, the 300 °C has smaller absorption range with a bandgap energy of 3.04 eV and the 400 °C has the smallest absorption range with a bandgap energy of 3.12 eV. Another research team [14] has also investigated the absorption range of C-doped TiO_2 calcined at 400 °C, 500 and 600 °C, proving with the calcination

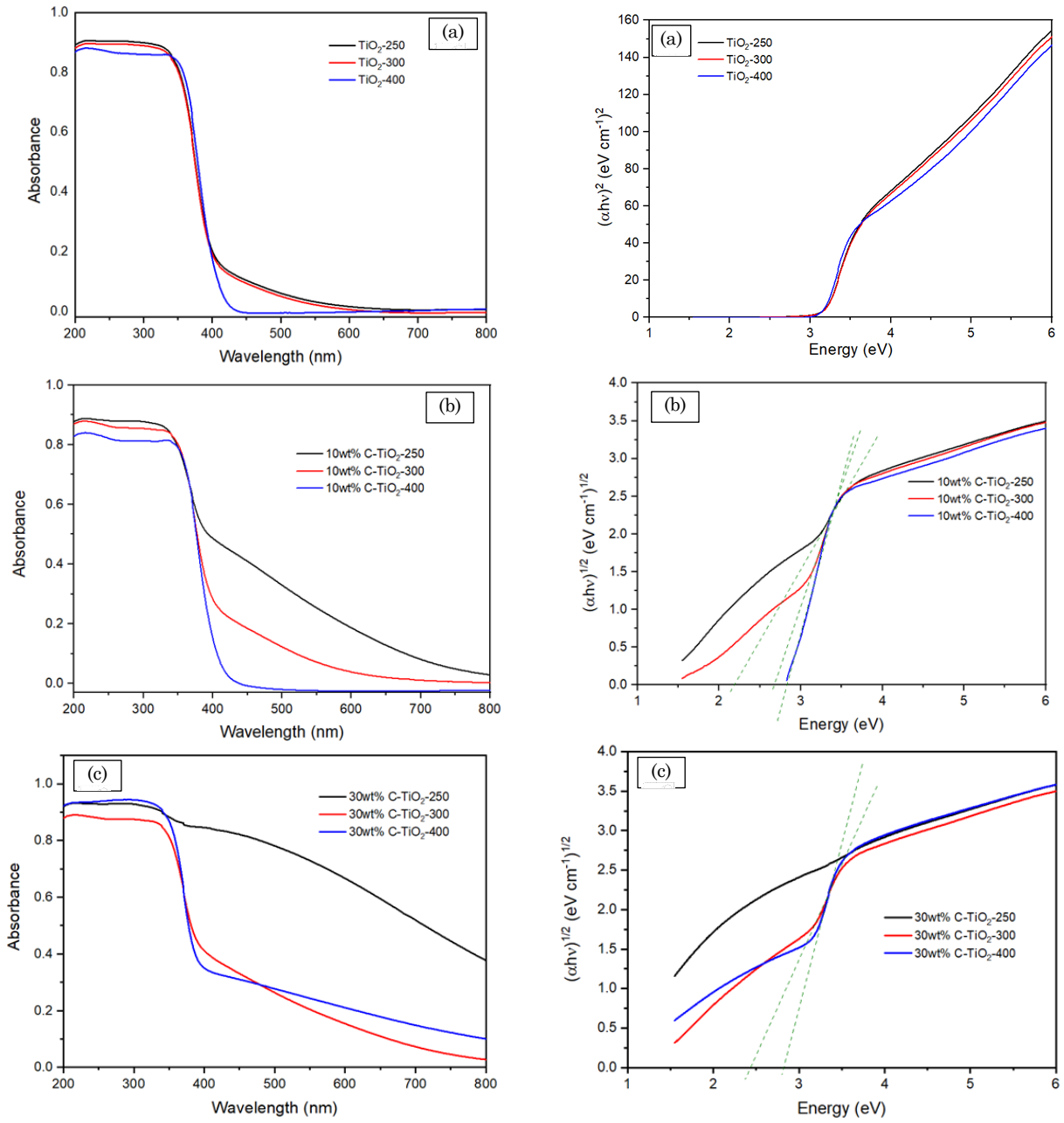

Figure 8. The diffuse reflectance spectra and the Kubelka-Munk plots for (a) undoped TiO_2, (b) 10wt%C-doped TiO_2, and (c) 30wt%C-doped TiO_2 at the calcined temperature of 200, 300, and 400 °C.

temperature increases, the absorption range decreases. This indicates that the surface carbonate species could be oxidized at higher temperatures, and the doped carbon could also be driven out as a result of calcination. This is further be proven by our study that FTIR patterns show lower transmittance intensities for carbonaceous materials of 10wt%C-TiO_2 calcined at 300 and 400 °C. Therefore, the band gap energy of same carbon doping content increases with calcination temperature, resulting from the elimination of carbon from the lattice of TiO_2 when the calcination temperature increases.

Based on Table 2, the bandgap energy of the undoped TiO_2-250, TiO_2-300, and TiO_2-400 are recorded as 2.8699 eV, 2.8823 eV, and 2.8610 eV, respectively, by the intercept plots of the $(\alpha h\upsilon)^{1/2}$ versus photon energy ($h\upsilon$). The bandgap energy of 10wt%C-TiO_2-250, 10wt%C-TiO_2-300, and 10wt%C-TiO_2-400 are 2.1606 eV, 2.6797 eV, and 2.8262 eV. The bandgap energy of 30wt%C-TiO_2-300 and 30wt%C-TiO_2-400 are recorded as 2.4913 eV and 2.6886 eV. Figure 7(a) and (b) also show no steep slope for the Kubelka-Munk plot of 50wt%C-TiO_2-250 and 50wt%C-TiO_2-300, thus their bandgap energies are undefined as well. Fortunately, under a higher calcination temperature, the bandgap energy of 50wt%C-TiO_2-400 could be determined, that is 2.2744 eV. The undefined band gaps might be due to the relatively high carbon content and low calcination temperature. Since carbon content is not semiconductor, thus excessive amounts that doped TiO_2 would cause the ultraviolet light and visible light cannot be absorbed by C-doped TiO_2 to cause electron excitation. To resolve the light hindrance caused by excessive carbon dopants, a higher calcination temperature could be used to partially decompose the carbon content on TiO_2.

The 30wt%C-TiO_2-300 has the highest photodegradation efficiency, which might be attributed by its narrower bandgap energy of 2.6797 eV. The lesser energy is needed for photogenerated electrons to jump from the valence band to the conduction band and create more electron-hole pairs at a narrower band gap. However, a very narrowed band gap (< 2.6 eV) makes electron-hole pairs recombine fast and thus, reducing effective photogenerated electrons to move to the catalyst surface and then, generating reactive oxygen species (ROS). Hence, the bandgap energy of 2.6797 eV is the optimum bandgap energy in our study, which has high free carriers' generation rate and low free carrier recombination rate.

Table 2. The band gap energy of undoped TiO_2 and C-doped TiO_2.

No.	Photocatalysts	Bandgap energy (eV)
1	TiO_2-250	2.8699
2	10wt%C-TiO_2-250	2.1606
3	30wt%C-TiO_2-250	-
4	50wt%C-TiO_2-250	-
5	TiO_2-300	2.8823
6	10wt%C-TiO_2-300	2.6797
7	30wt%C-TiO_2-300	2.4913
8	50wt%C-TiO_2-300	-
9	TiO_2-400	2.8610
10	10wt%C-TiO_2-400	2.8262
11	30wt%C-TiO_2-400	2.6886
12	50wt%C-TiO_2-400	2.2744

3.3 XRD Characterizations

3.3.1 Effects of calcination temperatures on carbon-doped TiO_2

Figure 9 presents the XRD patterns of carbon modified TiO_2 synthesized by the solvothermal-calcination method at different calcination temperature (250, 300, and 400 °C) and carbon loading percentage (10, 30, and 50 wt%). The synthesized carbon doped TiO_2 shows only anatase with higher photocatalytic activity as the calcination temperature is controlled under the phase transition temperature ranging from 500 to 600 °C [14]. The (101) plane is mainly discussed in this report as it is the more obvious peak and more representative than other planes. Doping with carbon slows down the phase transition and provides better crystallization of TiO_2 [20]. The crystallite size at the anatase peak (101) was calculated from the half-maximum peak with full width based on Scherrer equation ($D = \frac{K\lambda}{\beta \cos\theta}$).

Table 3 shows the crystallite size at different calcination temperature and the size increases from 250 to 300 °C and decreases from 300 to 400 °C consistently at 3 different groups of carbon content. The particle growth and agglomeration are dominant to the crystallite size when the temperature increases from 250 to 300 °C due to

Table 3. The crystallite sizes of undoped TiO_2 and C-doped TiO_2 in comparison of calcination temperature given the same carbon content.

Photocatalyst	Crystallite size (nm)
Undoped TiO_2	8.51
10wt%C-TiO_2-250	4.48
10wt%C-TiO_2-300	8.18
10wt%C-TiO_2-400	6.97
30wt%C-TiO_2-250	6.44
30wt%C-TiO_2-300	7.73
30wt%C-TiO_2-400	7.03
50wt%C-TiO_2-250	5.56
50wt%C-TiO_2-300	6.49
50wt%C-TiO_2-400	5.74

the nucleation rate and crystallization rate are increased with the supplying thermal energy. This result agrees well with previous works that the size is increased with calcination temperature [14,21]. However, the size decreases with temperature ranging from 300 to 400 °C as the doped carbon is released from the structure. The carbon doping is inhibited at high calcination temperature, which is confirmed by weaker intensity of C–H bending in Figure 6(d) caused by the removal of doped carbon content in C-doped TiO_2. Nonetheless, another evidence is that the absence of Ti–C bond in XRD patterns reported by other research team [19]. Additionally, higher energy consumption during the calcination process is not favorable in terms of environmental conservation and production expense. The calcination temperature at 300 °C is the optimal choice with the largest crystallite size and facilitated electron transfer with varied carbon doping content to improve the photodegradation performance.

3.3.2 Effects of carbon loadings on carbon-doped TiO_2

Figure 10 shows the XRD patterns in varied carbon loadings of 10, 30, and 50 wt% at 250, 300, and 400 °C. Figures 10(a)–(c) shows similar XRD patterns of diffraction intensities and planes. The amplified XRD patterns at 300 °C is demonstrated in Figure 10 (d), where the (101) diffraction peak shifts to smaller 2θ and narrows, implying the carbon has been noticeably doped into the TiO_2 structure. The intensity increases with carbon loading at their corresponding fixed temperatures, except 10wt%C-TiO_2-400, caused by high calcination has almost burnt out the relatively low amount of carbon. The carbon doping contributes to higher crystallinity to provide synergistic effects on extending the absorption to visible light and accelerating the electron-hole separation [22].

The crystallite size is evaluated based on Scherrer equation and summarized in Table 4. It is found that the undoped TiO_2 has a crystallite size of 8.51 nm, while all the carbon doped TiO_2 has a smaller crystallite size range, 4.48–8.18 nm. At 300 °C calcination temperature, the crystallite sizes are decreasing from 8.18 to 6.46 nm with increasing of carbon loading, which is contributed by the inhibition of growth and aggregation of TiO_2 by carbon materials, and the same result is presented in previous researches [23,24]. While

Table 4. The crystallite sizes of undoped TiO_2 and C-doped TiO_2 in comparison of carbon content given the same calcination temperature.

Photocatalyst	Crystallite size (nm)
Undoped TiO_2	8.51
10wt%C-TiO_2-250	4.48
30wt%C-TiO_2-250	6.44
50wt%C-TiO_2-250	5.56
10wt%C-TiO_2-300	8.18
30wt%C-TiO_2-300	7.73
50wt%C-TiO_2-300	6.49
10wt%C-TiO_2-400	6.97
30wt%C-TiO_2-400	7.03
50wt%C-TiO_2-400	5.74

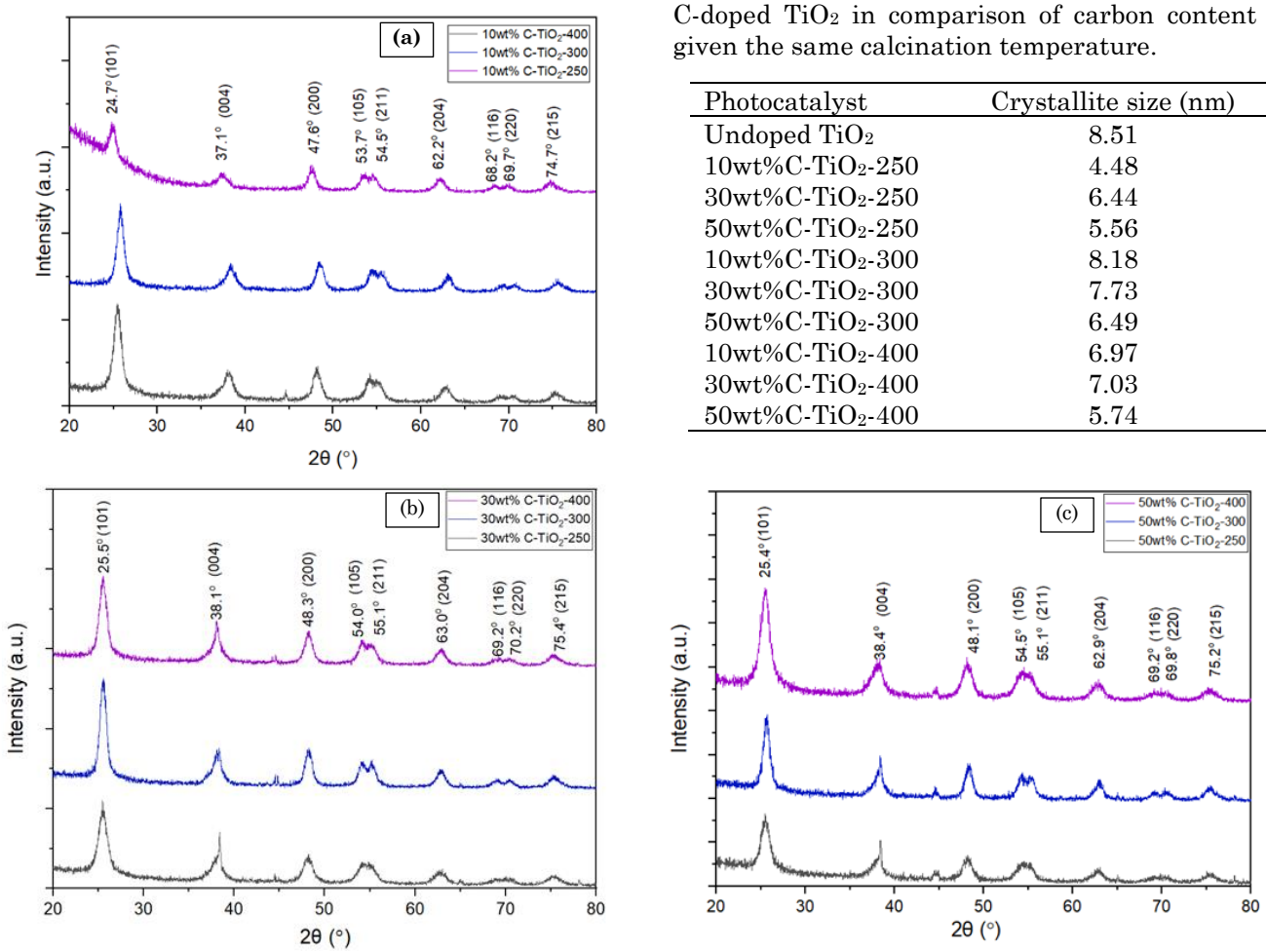

Figure 9. XRD diffractogram of different calcination temperatures of carbon-doped TiO_2 with carbon loadings at (a) 10 wt%, (b) 30 wt%, and (c) 50 wt%.

the abnormal tendency is observed in 250 and 400 °C where the crystallite size increases from 10 wt% carbon doping to 30 wt% and decreases from 30 wt% to 50 wt%. The crystallite sizes increase from 10 wt% to 30 wt% is mainly determined by the longer bond length of Ti-C compared with Ti-O with the loading of carbon, and it is the controlling factor in this temperature range [25]. Meanwhile, the crystallite sizes decrease from 30 wt% to 50 wt% is attributed by sufficient carbon content to inhibit the crystal growth. However, excessive residual doping carbon could obstruct the active surface towards light source thus decelerate the photogenerated electron-hole separation [26,27]. This result confirms that 30 wt% carbon loading surpasses the other loading percentage leading to an enhanced charge transfer and outstanding degradation activity.

3.4 Photoluminescence (PL) Characterization

3.4.1 Effects of calcination temperature towards charge transfer

As the XRD analysis solely verifies the incorporation of carbon into the crystallite structure through the degree shift, Photoluminescence (PL) is further carried to determine the effect of calcination temperature and carbon loading content on the vacancy generation and recombination rate. PL spectra at different calcination temperature are shown in Figure 11, where the lower intensity implies lower recombination rate and better separation and transfer of electrons. Three peaks are generally observed in PL spectra which encompass self-trapped excitons (420-430 nm) [20,28], surface oxygen vacancy (520-548 nm) [16,29] and bulk oxygen vacancy (590-640 nm) [30]. The surface oxygen vacancy is the most obvious and influencing factor for the photodegradation activity, hence the peak among the wavelength range of 520 to 540 nm is focused for discussion.

The similar trend is observed in Figures 11 (a) and (b) that the intensities decrease from 250 to 300 °C and increase from 300 to 400 °C, which indicating the lowest recombination rate and highest activity at 300 °C, in alignment with the result in Table 5. The high recombination rate at 250 °C is attributed by the insufficient carbon doping at low calcination temperature; thus, the electron trapping is deficient. Besides, most of the doped carbon is released from the crystallite structure at 400 °C, hence carbon is lacking to inhibit the recombination of electron-hole pairs [27]. The highest activity in 300 °C ensures the desirable performance with sufficient surface oxygen vacancy and high electron transfer efficiency.

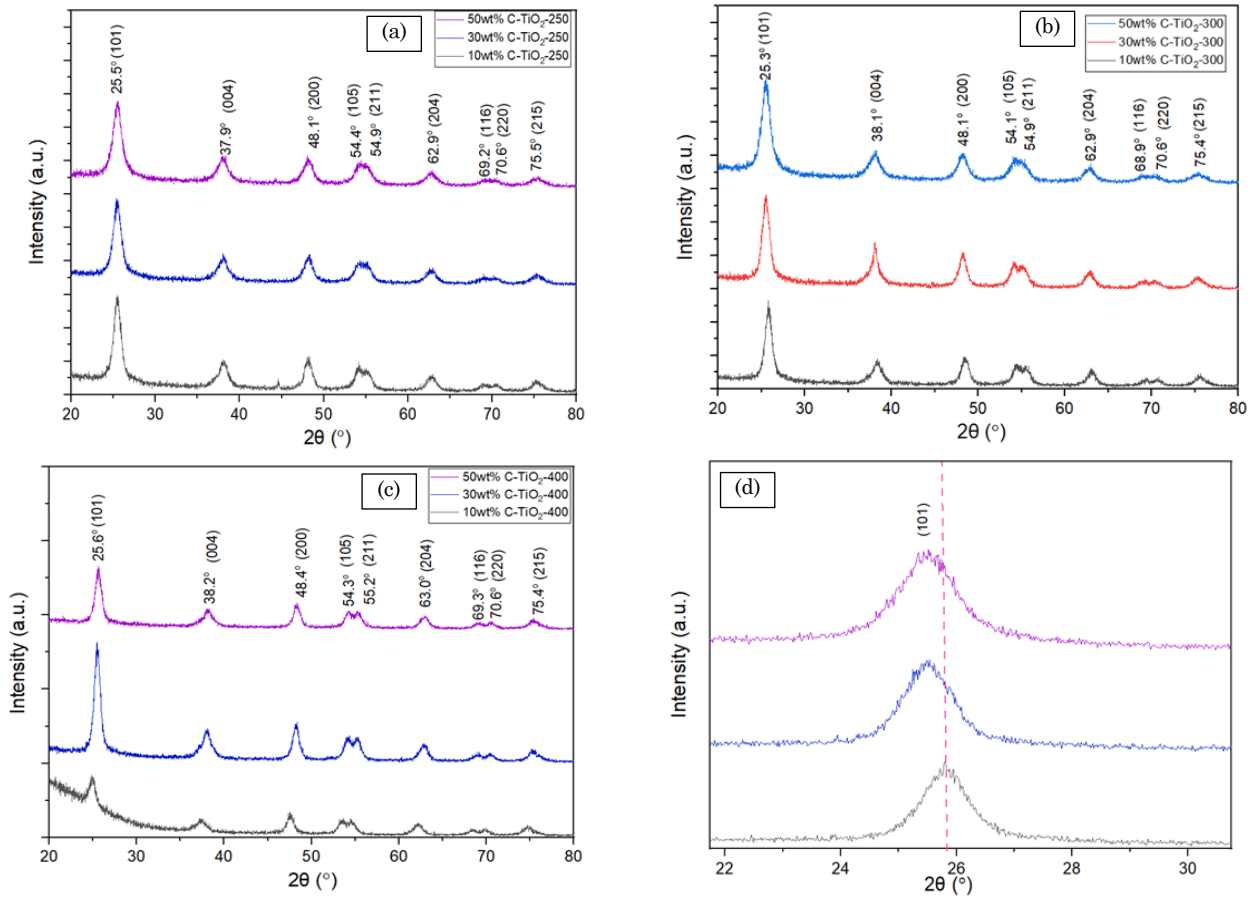

Figure 10. XRD diffractogram of varied carbon loadings of carbon-doped TiO_2 at (a) 250 °C, (b) 300 °C, and (c) 400 °C

3.4.2 Effects of carbon loadings towards charge transfer

Figure 12 displays the PL spectra at different amount of carbon loadings, and the intensities increase with carbon loadings at three groups with varied calcination temperatures. The undoped TiO_2 shows the highest intensity and largest recombination rate, therefore, carbon doping is confirmed to retard the recombination and accelerate electron transfer. Besides, the intensity increases continually from 10 wt% to 50 wt% which is consistent to past researches [31,32]. This phenomenon is caused by the suppressed electron mobility at higher carbon content in the crystallite structure. Furthermore, the defects in lattice introduce recombination channel formed by free electrons, thus the emission efficiency and photodegradation activity are decreased with larger amount of carbon is doped into the structure [33]. This result suggests the 10 wt%

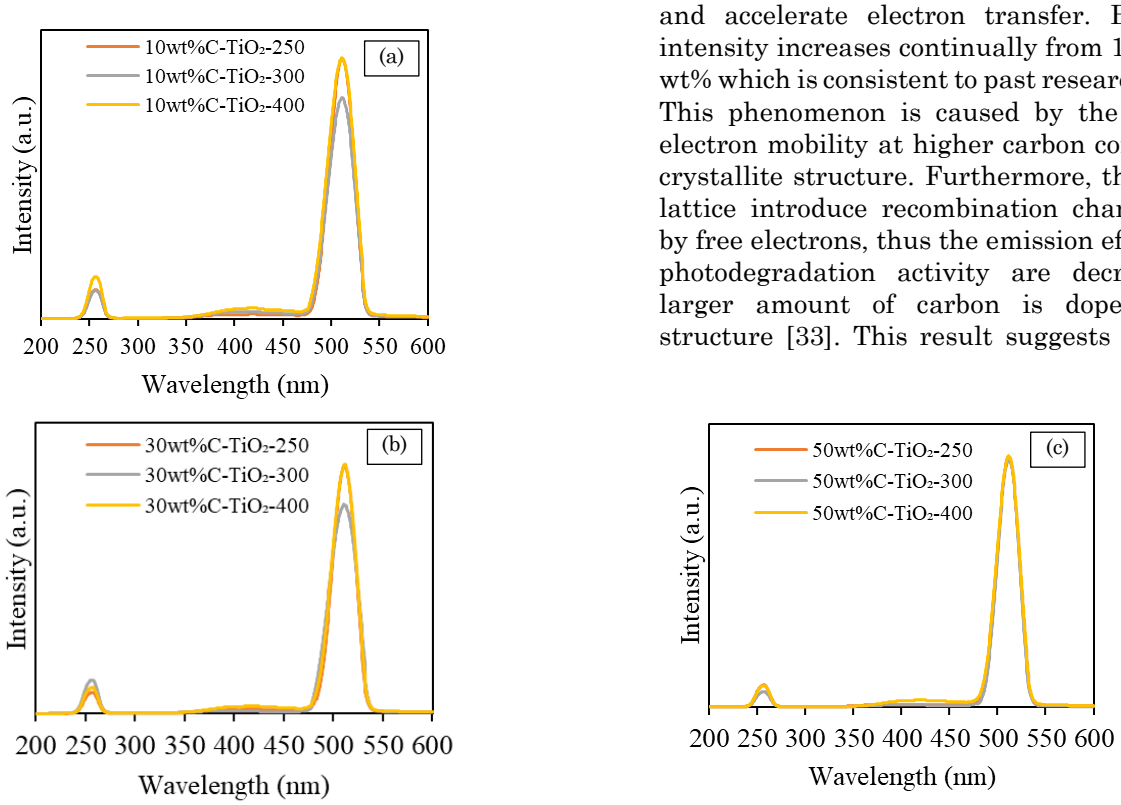

Figure 11. PL spectra of different loadings amount of citric acid in carbon-doped TiO_2 at (a) 10 wt%, (b) 30 wt%, and (c) 50 wt%.

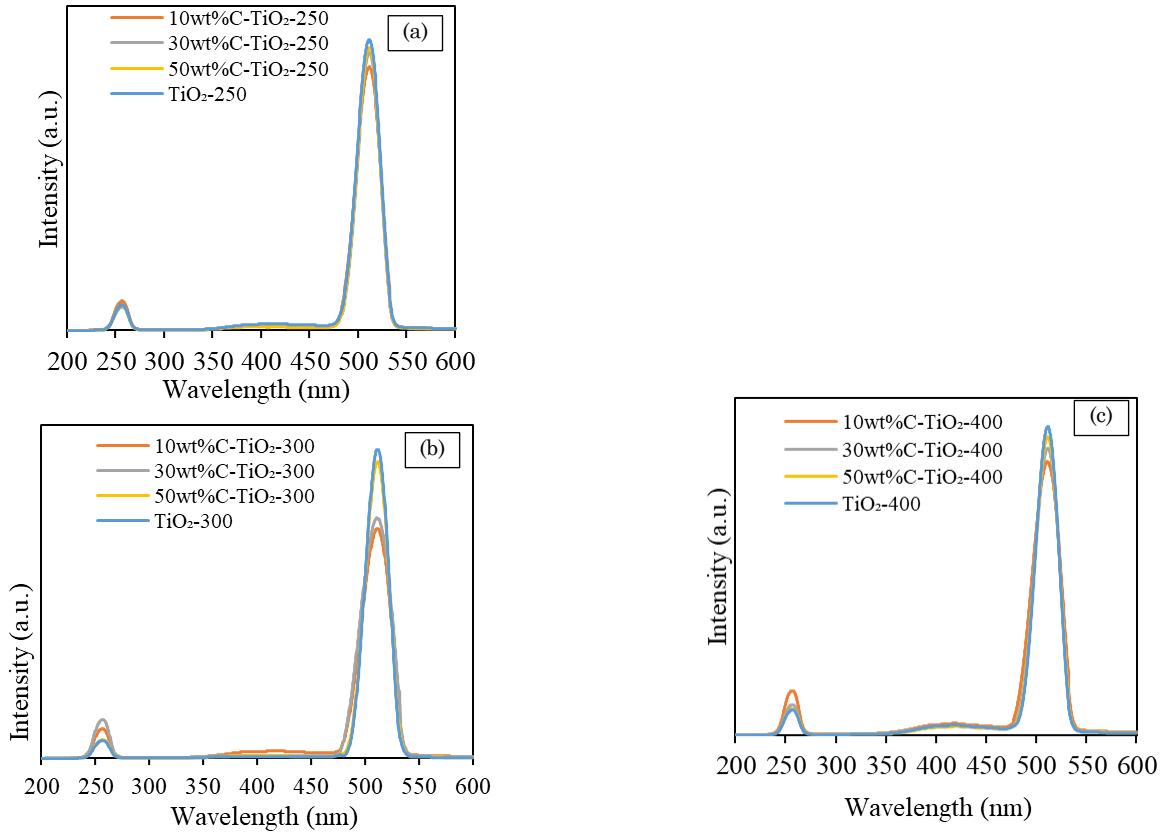

Figure 12. PL spectra of different loadings amount of citric acid in carbon-doped TiO_2 at (a) 10 wt%, (b) 30 wt%, and (c) 50 wt%.

carbon loading is the optimal composition in terms of activity and cost efficiency of photocatalyst production.

3.5 Photocatalytic Activity

The photodegradation removal efficiency (%) of all synthesized catalysts were carried out. All of the experiments adopted 0.1 g catalysts, 5 mmol H_2O_2 and 25 ppm MO at pH = 3.3 under 300 rpm stirring. Owing to MO is an anionic dye, it prefers to combine with the cations, so it prefers to degrade under the acid environment. The acid provides H^+ ion, making the surface of TiO_2 becoming positive to adsorb more anionic ions to improve photodegradation removal efficiency (%). And the H_2O_2 is the oxidant which can provide ·OH. He *et al.* [34] used a WO_3/TiO_2 combination film to study the photocatalytic activity in relation to pH and other inorganic anions and found that the removal efficiency decreased as pH increased, and anions such as PO_4^{3+}, NO_3^+ and HCO_3^+ will interact with water to form ·OH to help remove MO and the anions such as Cl^- and SO_4^{2+} will trap the ·OH to inhibit the elimination of MO. Therefore, use H_3PO_4 to regulate pH value.

Figure 13 shows the effect of carbon doping amount on photocatalyst activity. When the photocatalysts were calcined at 250, 300, and 400 °C, the degradation rates of MO increase first and then decrease with increasing of carbon content from 0 to 50%. All of the C-doped TiO_2, except 50wt%C-TiO_2-400, has higher photoactivity than undoped TiO_2 in the same calcination temperature, respectively. The high photocatalytic activity might be owing to the carbon interpolates into the lattice of the TiO_2 and creates a new energy level above the valence band to narrow the bandgap, making electrons easy to be excited. Park *et al.* [19] found that the surface carbonaceous materials on TiO_2 would be oxidized into CO_2 through photocatalysis under UV irradiation which inhibit the pollutant degradation. And after 1 hour UV light irradiation, the photoactivity of catalyst slightly decreased, but further did not decrease means that the photoactivity largely ascribed to the presence of doped carbon. Therefore, a certain amount of carbonaceous materials coating helps to adsorb pollutants and too much surface carbonaceous materials inhibit the photodegradation. Hence, 50 wt% carbon doped TiO_2 always have the lowest photoactivity.

Among them, 10wt%C-TiO_2-300 has the highest photocatalytic activity, and the final photodegradation removal efficiency of 62.1% can be obtained under 2 h of light irradiation. The band gap energy of the 10wt%C-TiO_2-300 is 2.6767 eV, which is the optimum band gap energy. It needs less energy to excite the photogenerated electrons and has low recombination rate of charge carriers. The 30wt%C-TiO_2-400 has a similar bandgap energy, 2.6886 eV, as 10wt%C-TiO_2-300, but its photodegradation removal efficiency is 48.94%, which was less than 62.1%, possibly caused by the dopant level acts as recombination center at a higher dopant concentration. 50wt%C-TiO_2-400 has the lowest activity due to its high recombination rate shown by PL results. Under the high calcination temperature, the carbonaceous materials on the surface will be eliminated and thus, reducing the adsorption ability of MO onto catalyst surface. In

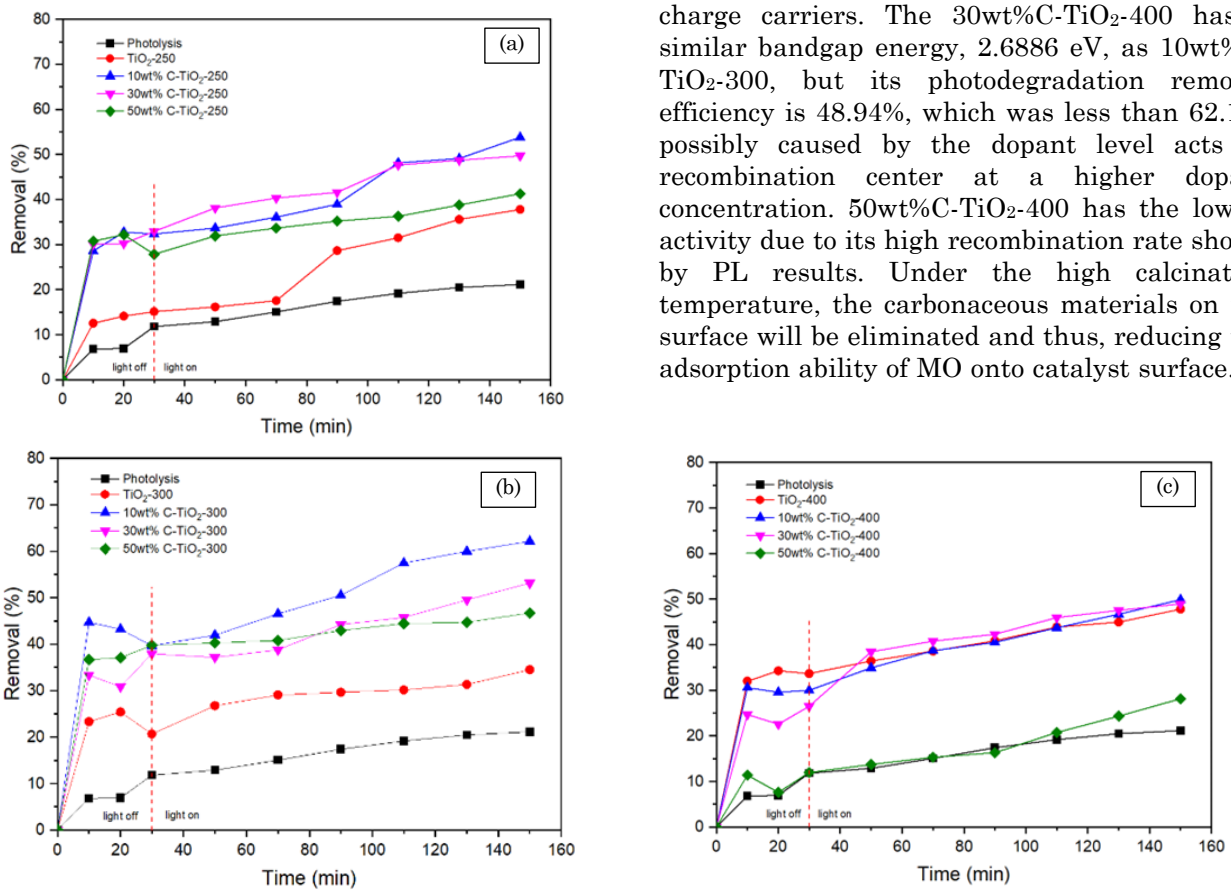

Figure 13. Effect of the carbon concentration of CA-TiO_2 under (a) 250 °C, (b) 300 °C, (c) 400 °C calcination on the photocatalytic efficiency of MO

addition, the dopant level generated by high carbon dopant concentration will provide more recombination centers compared to charge carriers, hence, reducing the electron charge transfer for MO photodegradation.

Figure 14 shows that under the sample carbon dopant concentration, the photocatalysts calcined under 300 °C always have the highest photodegradation efficiency and the photocatalysts calcined under 400 °C always have the lowest photodegradation efficiency. C-doped TiO_2 calcined under 250 °C has lower activity than C-doped TiO_2 calcined under 300 °C may because of larger band gap and faster recombination rate. C-doped TiO_2 calcined under 400 °C has lower photoactivity than C-doped TiO_2 calcined under 250 and 300 °C because of the elimination of carbonaceous materials on the surface could cause less MO adsorption. Table 5 summarizes the undoped TiO_2 and C-doped TiO_2 in photodegradation of MO pollutant.

The photodegradation effect of 10wt%C-TiO_2-300 are shown in Figure 15. The results were collected on the initial concentration (before photodegradation), dark condition (after 30 minutes), and every 20 minutes after illumination. It can be clearly seen that the color of MO becomes lighter with the increase of illumination time, which proves that C-doped TiO_2 is effective for photodegradation, and the longer the illumination time, the better the effect.

According to Table 6, 10wt%C-TiO_2-300 shows relatively good photodegradation removal efficiency rate 0.52%/min, which is comparable with other photocatalysts which gave better performance at a higher power (500 W) and lower pollutant concentrations (below 10 ppm). 10wt%C-TiO_2-300 is a good photoactivity and energy efficient photocatalyst as lower power (100 W) was irradiated at high concentration of pollutant (25 ppm) in a short photocatalytic degradation period (2 h).

3.6 Mechanistic Pathways

Past studies have focused on the alkane and polyol organic compounds, such as hexane, heptane, and glucose, as the doping agents to narrow the wide band gap of TiO_2 (approx. 3.2 eV). This TiO_2 wide band gap is a limitation as it utilizes a higher energy consumption (UV light). Doping with the aforementioned carbon materials, the band gap can be narrowed, and the

Table 5. Photodegradation removal efficiency of MO

Photocatalyst	Photodegradation (%)
Photolysis	21.10
TiO_2-250	37.77
10wt%C-TiO_2-250	53.80
30wt%C-TiO_2-250	49.65
50wt%C-TiO_2-250	41.28
TiO_2-300	34.48
10wt%C-TiO_2-300	62.10
30wt%C-TiO_2-300	53.16
50wt%C-TiO_2-300	46.72
TiO_2-400	47.80
10wt%C-TiO_2-400	49.87
30wt%C-TiO_2-400	48.94
50wt%C-TiO_2-400	28.11

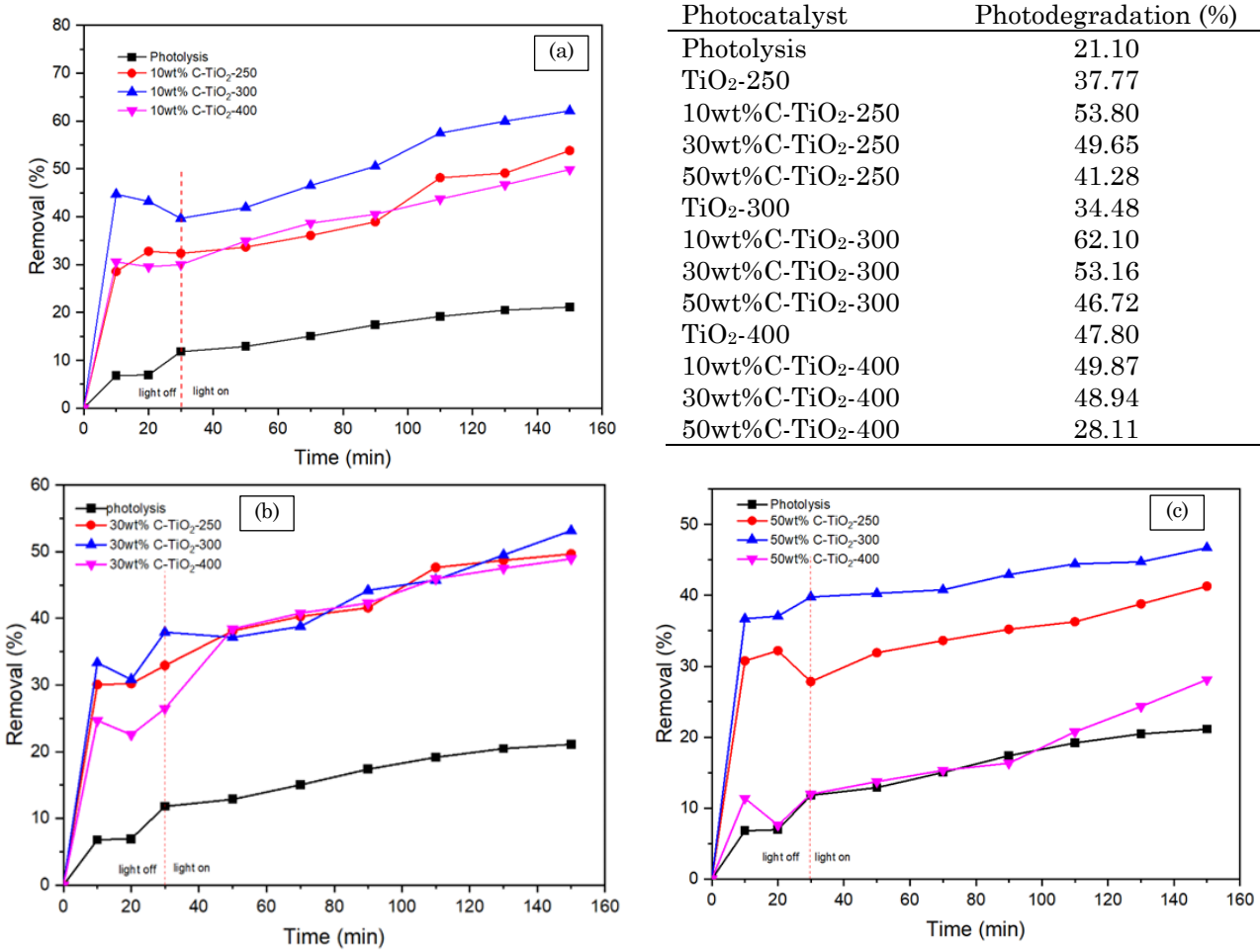

Figure 14. The Effect of the calcination temperature of CA-TiO_2 under (a) 10 wt%, (b) 30 wt%, (c) 50 wt% dopant concentration on the photocatalytic efficiency of MO.

absorption band can be extended to a longer wavelength (visible light region).

Up to date, lack of findings on utilizing the carboxylic acid-based compounds to modify the TiO_2. Thus, carboxylic acid, citric acid, is used to dope with TiO_2. Citric acid is a bio-based material widely found in nature and highly accessible. The doping approach aims to incorporate the carbon into the interstitial of TiO_2, then form Ti–O–C structure and narrow the TiO_2 wide band gap (<3.2 eV). Withal, the citric acid's carboxyl group (-COOH) will partially modify the TiO_2 surface after the calcination, and withdrawing the photogenerated electrons at the conduction band. Subsequently, the process enhances the charge separation and interfacial transfer. By preventing the charge recombination with the photogenerated holes at the valence band, more hydroxyl radicals can be generated by H_2O_2 reduction. Ultimately, the photodegradation is expected to be improved.

Furthermore, the addition of the carbon source can decrease the calcination temperature. It is due to incorporating the dissociated anions, COO^-, from citric acid into the TiO_2. The affinity of anions, COO^-, plays a vital role in phase transformation. The weaker affinity of anions to Ti^{4+} within the TiO_2, the easier the rearrangement of TiO_6 moieties. Therefore, the weak affinity of carbon ions improved the structure rearrangement, subsequently, the phase transformation. Thus, if the concentration of carbon increases, in other words, more carbon ions are introduced, the anatase to rutile phase transformation temperature decreased.

Below is a schematic illustration of reaction mechanism of C-doped TiO_2 (Figure 16). First, the C-doped TiO_2 is illuminated by the visible light and absorbs the energy of hv, then the electron – hole pairs were generated in the TiO_2 lattice. The photogenerated electron in the conduction band will capture O_2 to produce $^{\bullet}O_2^-$. The $HO_2^{\bullet}$ is produced by the protonation of $^{\bullet}O_2^-$ and it will combine the electrons to generate H_2O_2. The H_2O_2 will produce the $OH^{\bullet}$ radicals which are the most oxidizing species. What's more, the holes will combine with the OH^- to generate more $OH^{\bullet}$ radicals. Finally, the $OH^{\bullet}$ radicals will react with methyl orange and degrade it. Please refer to Equations (3) – (12).

4. Conclusions

In this study, the C-doped TiO_2 was synthesized to study their properties and photoactivity. The C-doped TiO_2 with 10 wt%, 30 wt% and 50 wt% dopant concentration was produced by using citric acid as carbon source with the solvent-calcination method. The synthesized catalysts were calcined with low temperature at 200, 300, and 400 °C. Finally, get the yellow or brown color C-doped TiO_2 catalysts which suggests that the carbon had doped into the TiO_2. DR UV-Vis and FT-IR were used to characterize the properties of the C-doped TiO_2. All the synthesized C-doped TiO_2 had narrower bandgap energy than undoped TiO_2. These results prove that the carbon doped into the lattice of TiO_2 to create a new energy level above the valence band

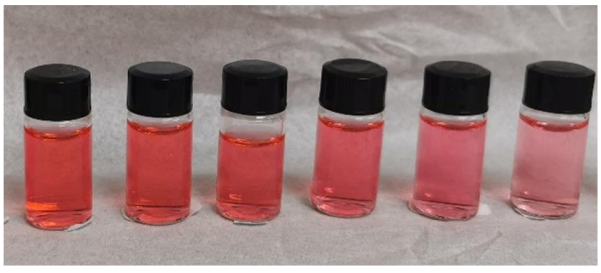

Figure 15. The photodegradation effect of CA-TiO_2-10 wt%-250 with 2 hours irradiation

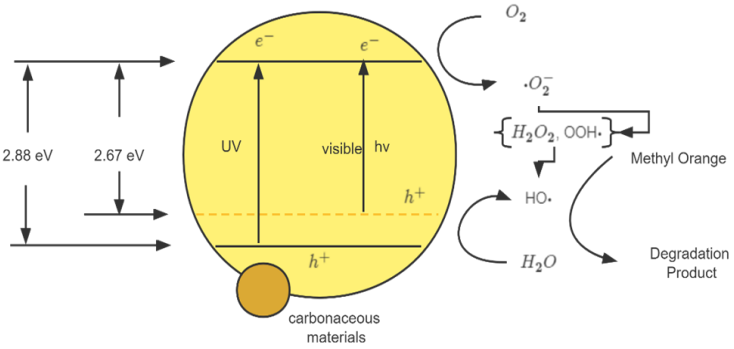

Figure 16. Plausible schematic illustration of reaction mechanism of C-doped TiO_2

Table 6. Comparisons analogous carbon-doped TiO_2 photocatalysts

Catalyst	Calc. temp. (°C)	Lamp	Lamp power (W)	Catalyst loading (g/mL)	Pollutant conc. (ppm)	Irradiation time (min)	Photodegrad. removal efficiency (%)	Photodegrad. removal efficiency rate (%/min)	Ref.
10wt%C-TiO_2-300	300	Xe lamp	100	0.1/500	25	120	62.1	0.52	Our work
TA_2-500	500	UV light	40	0.5/200	1	100	89	0.89	[35]
2% C/TiO_2	500	Xe lamp	300	0.1/100	0.2	120	100	0.83	[36]
0.04 wt% C-TiO_2	200	sunlight	753	0.06/250	10	180	97	0.53	[13]

to narrow the bandgap making the electrons easier to excite. The FT-IR spectra of C-doped TiO_2 show the -OH stretching, -OH bending vibration, C-H and Ti-O stretching band. The appearance of the C-H band means that the carbonaceous materials existed on the surface of the C-doped TiO_2. It is found that the undoped TiO_2 has a crystallite size of 8.51 nm while C-doped TiO_2 has a smaller crystallite size range, 4.48–8.18 nm, which is contributed by the inhibition of growth and aggregation of TiO_2 by carbon contents. Contrarily, the crystallite sizes increase with heightening of calcination temperature due to thermal energy enhances the crystal growth. Notably, C-doped TiO_2 exhibits anatase phase as the calcination temperature is well controlled within 250 to 400 °C, moreover, the carbon content could inhibit the phase transformation as well. The surface oxygen vacancy is the key factor for the photodegradation activity, which the optimized electron trappers have been generated at 300 °C by adopting 10wt% C-doped TiO_2. Except the 50wt%C-TiO_2-400, all C-doped TiO_2 showed better photodegradation results than the undoped TiO_2 under the same calcination temperature. Among all the synthesized photocatalysts, the 10wt%CA-TiO_2-300 showed the best photodegradation efficiency, 62.1% with the bandgap energy of 2.67 eV under 100 W illumination. To evaluate the influence of reactive species (•OH, $•O_2^-$, h^+) on photocatalysis using C-doped TiO_2, quenching experiments with isopropanol or tert-butanol (a •OH radical scavenger), potassium iodide or Na_2EDTA (a h^+ scavenger), and nitrotetrazolium blue chloride or *p*-benzoquinone (an $•O_2^-$ radical scavenger) will be adopted in future. Overall, the experiment outputs provide future possibilities of this energy efficient carbon-doped TiO_2 in the treatment of textile wastewater under visible light irradiation.

Acknowledgment

The work is supported by Xiamen University Malaysia Research Fund (grant number: XMUMRF/2019-C4/IENG/0019 and XMUMRF/2020-C5/IENG/0029). The authors would like to thank the laboratory executives and officers, including Dr. Nur Dalila binti Mohamad, Ms. Nurul Aida binti Sulaiman, Ms. Siti Najihah binti Md Hashim, Mr. Mohd Zulhelmy bin Ahmad, and Ms. Nur Izzati Binti Mohd Razali, for providing technical support, which greatly contributed to the success of this research.

Statements and Declarations

The authors declare that they have no known competing financial interests or personal relationships that could have appeared to influence the work reported in this paper.

CRedit Author Statement

Xinying Han: Investigation, Project administration, Validation; Visualization, Writing - original draft; Yubei Guo: Validation, Writing - original draft; Chien Yong Goh: Data curation, Writing - review & editing; Cheng Loong Ngan: Conceptualization, Writing - review & editing; Jian Ping Tan: Resources, Writing - review & editing; Peng Chee Tan: Resources, Writing - review & editing; Abdulkareem Ghassan Alsultan: Conceptualization, Resources; Yun Hin Taufiq-Yap: Conceptualization, Resources; Sin Yuan Lai: Funding acquisition, Methodology, Supervision, Resources, Writing - review & editing. All authors have read and agreed to the published version of the manuscript.

References

[1] Guo, H., Jiang, S., Wang, C., Li, S., Feng, J., Sun, H., Zhu, H., Guo, H., Liu, M., Sun, H. (2019). Carbonaceous Nanofibers-titanium Dioxide Nanocomposites: Synthesis and Use as a Platform for Removal of Dye Pollutants. *Journal Wuhan University of Technology, Materials Science Edition*, 34(2), 303–307. DOI: 10.1007/s11595-019-2051-9.

[2] Shen, S., Li, H., Fu, J. jia, Wang, H.B. (2022). Wastewater purification with different precursors of carbon dots dominated titanium dioxide: Mechanism insight. *Journal of Alloys and Compounds*, 922, 166162. DOI: 10.1016/j.jallcom.2022.166162.

[3] Al-Mamun, M.R., Kader, S., Islam, M.S., Khan, M.Z.H. (2019). Photocatalytic activity improvement and application of UV-TiO2 photocatalysis in textile wastewater treatment: A review. *J. Environ. Chem. Eng.* 7, 103248. DOI: 10.1016/j.jece.2019.103248.

[4] Samadi, A., Gao, L., Kong, L., Orooji, Y., Zhao, S. (2022). Waste-derived low-cost ceramic membranes for water treatment: Opportunities, challenges and future directions. Resour. Conserv. Recycl. 185, 106497. DOI: 10.1016/j.resconrec.2022.106497.

[5] Moslah, C., Kandyla, M., Mousdis, G.A., Petropoulou, G., Ksibi, M. (2018). Photocatalytic Properties of Titanium Dioxide Thin Films Doped with Noble Metals (Ag, Au, Pd, and Pt). *Physica Status Solidi (A) Applications and Materials Science*, 215(17), 800023. DOI: 10.1002/pssa.201800023.

[6] Astuti, Y., Musthafa, F., Arnelli, A., Nurhasanah, I. (2022). French Fries-Like Bismuth Oxide: Physicochemical Properties, Electrical Conductivity and Photocatalytic Activity. *Bulletin of Chemical Reaction Engineering & Catalysis*, 17(1), 146–156. DOI: 10.9767/BCREC.17.1.12554.146-156.

[7] Nasralla, N., Yeganeh, M., Astuti, Y., Piticharoenphun, S., Shahtahmasebi, N., Kompany, A., Karimipour, M., Mendis, B.G., Poolton, N.R.J., Šiller, L. (2013). Structural and spectroscopic study of Fe-doped TiO2 nanoparticles prepared by sol-gel method. *Scientia Iranica*, 20(3), 1018–1022. DOI: 10.1016/j.scient.2013.05.017.

[8] Astuti, Y., Ana Tasiman, B.H., Widiyandari, H., Arutanti, O., Mufti, N., Ogi, T. (2024). A mixed Bi2O3/CQDs provides better photocatalytic activity in organic dyes pollutant model. *Nanotechnology for Environmental Engineering*. 9, 561–571. DOI: 10.1007/s41204-024-00383-8

[9] Xu, C., Killmeyer, R., Gray, M.L., Khan, S.U.M. (2006). Photocatalytic effect of carbon-modified n-TiO2 nanoparticles under visible light illumination. *Applied Catalysis B: Environmental*, 64(3–4), 312–317. DOI: 10.1016/j.apcatb.2005.11.008.

[10] Gómez-Avilés, A., Peñas-Garzón, M., Bedia, J., Rodriguez, J.J., Belver, C. (2019). C-modified TiO2 using lignin as carbon precursor for the solar photocatalytic degradation of acetaminophen. *Chemical Engineering Journal*, 358, 1574–1582. DOI: 10.1016/j.cej.2018.10.154.

[11] Dong, F., Wang, H., Wu, Z. (2009). One-step "Green" synthetic approach for mesoporous C-doped titanium dioxide with efficient visible light photocatalytic activity. *Journal of Physical Chemistry C*, 113(38), 16717–16723. DOI: 10.1021/jp9049654.

[12] Janus, M., Tryba, B., Inagaki, M., Morawski, A.W. (2004). New preparation of a carbon-TiO2 photocatalyst by carbonization of n-hexane deposited on TiO2. *Applied Catalysis B: Environmental*, 52(1), 61–67. DOI: 10.1016/j.apcatb.2004.03.011.

[13] Kavitha, R., Devi, L.G. (2014). Synergistic effect between carbon dopant in titania lattice and surface carbonaceous species for enhancing the visible light photocatalysis. *Journal of Environmental Chemical Engineering*, 2(2), 857–867. DOI: 10.1016/j.jece.2014.02.016.

[14] Lin, Y.T., Weng, C.H., Lin, Y.H., Shiesh, C.C., Chen, F.Y. (2013). Effect of C content and calcination temperature on the photocatalytic activity of C-doped TiO2 catalyst. *Separation and Purification Technology*, 116, 114–123. DOI: 10.1016/j.seppur.2013.05.018.

[15] Xiao, Q., Zhang, J., Xiao, C., Si, Z., Tan, X. (2008). Solar photocatalytic degradation of methylene blue in carbon-doped TiO2 nanoparticles suspension. *Solar Energy*, 82(8), 706–713. DOI: 10.1016/j.solener.2008.02.006.

[16] Teng, F., Zhang, G., Wang, Y., Gao, C., Chen, L., Zhang, P., Zhang, Z., Xie, E. (2014). The role of carbon in the photocatalytic reaction of carbon/TiO2 photocatalysts. *Applied Surface Science*, 320, 703–709. DOI: 10.1016/j.apsusc.2014.09.153.

[17] Ma, Y., Han, L., Ma, H., Wang, J., Liu, J., Cheng, L., Yang, J., Zhang, Q. (2017). Improving the visible-light photocatalytic activity of interstitial carbon-doped TiO2 with electron-withdrawing bidentate carboxylate ligands. *Catalysis Communications*, 95, 1–5. DOI: 10.1016/j.catcom.2017.02.025.

[18] Wu, X., Yin, S., Dong, Q., Guo, C., Li, H., Kimura, T., Sato, T. (2013). Synthesis of high visible light active carbon doped TiO2 photocatalyst by a facile calcination assisted solvothermal method. *Applied Catalysis B: Environmental*, 142–143, 450–457. DOI: 10.1016/j.apcatb.2013.05.052.

[19] Park, Y., Kim, W., Park, H., Tachikawa, T., Majima, T., Choi, W. (2009). Carbon-doped TiO2 photocatalyst synthesized without using an external carbon precursor and the visible light activity. *Applied Catalysis B: Environmental*, 91(1–2), 355–361. DOI: 10.1016/j.apcatb.2009.06.001.

[20] Li, W., Liang, R., Zhou, N.Y., Pan, Z. (2020). Carbon Black-Doped Anatase TiO2 Nanorods for Solar Light-Induced Photocatalytic Degradation of Methylene Blue. *ACS Omega*, 5(17), 10042–10051. DOI: 10.1021/acsomega.0c00504.

[21] Chen, C., Long, M., Zeng, H., Cai, W., Zhou, B., Zhang, J., Wu, Y., Ding, D., Wu, D. (2009). Preparation, characterization and visible-light activity of carbon modified TiO2 with two kinds of carbonaceous species. *Journal of Molecular Catalysis A: Chemical*, 314(1–2), 35–41. DOI: 10.1016/j.molcata.2009.08.014.

[22] Wang, Y., Chen, Y.X., Barakat, T., Wang, T.M., Krief, A., Zeng, Y.J., Laboureur, M., Fusaro, L., Liao, H.G., Su, B.L. (2021). Synergistic effects of carbon doping and coating of TiO2 with exceptional photocurrent enhancement for high performance H2 production from water splitting. *Journal of Energy Chemistry*, 56, 141–151. DOI: 10.1016/j.jechem.2020.08.002.

[23] Lin, Y.T., Weng, C.H., Lin, Y.H., Shiesh, C.C., Chen, F.Y. (2013). Effect of C content and calcination temperature on the photocatalytic activity of C-doped TiO2 catalyst. *Separation and Purification Technology*, 116, 114–123. DOI: 10.1016/j.seppur.2013.05.018.

[24] Zhong, J., Chen, F., Zhang, J. (2010). Carbon-deposited TiO2: Synthesis, characterization, and visible photocatalytic performance. *Journal of Physical Chemistry C*, 114(2), 933–939. DOI: 10.1021/jp909835m.

[25] Raghu, A.V., Karuppanan, K.K., Pullithadathil, B. (2019). Controlled Carbon Doping in Anatase TiO2 (101) Facets: Superior Trace-Level Ethanol Gas Sensor Performance and Adsorption Kinetics. *Advanced Materials Interfaces*, 6(4) DOI: 10.1002/admi.201801714.

[26] Perera, S.D., Mariano, R.G., Vu, K., Nour, N., Seitz, O., Chabal, Y., Balkus, K.J. (2012). Hydrothermal synthesis of graphene-TiO2 nanotube composites with enhanced photocatalytic activity. *ACS Catalysis*, 2(6), 949–956. DOI: 10.1021/cs200621c.

[27] Gonçalves, B.S., Palhares, H.G., Souza, T.C.C.D., Castro, V.G.D., Silva, G.G., Silva, B.C., Krambrock, K., Soares, R.B., Lins, V.F.C., Houmard, M., Nunes, E.H.M. (2019). Effect of the carbon loading on the structural and photocatalytic properties of reduced graphene oxide-TiO2 nanocomposites prepared by hydrothermal synthesis. *Journal of Materials Research and Technology*, 8(6), 6262–6274. DOI: 10.1016/j.jmrt.2019.10.020.

[28] Sean, N.A., Leaw, W.L., Nur, H. (2019). Effect of calcination temperature on the photocatalytic activity of carbon-doped titanium dioxide revealed by photoluminescence study. *Journal of the Chinese Chemical Society*, 66(10), 1277–1283. DOI: 10.1002/jccs.201800389.

[29] Muniandy, L., Adam, F., Mohamed, A.R., Ng, E.P., Rahman, N.R.A. (2016). Carbon modified anatase TiO2 for the rapid photo degradation of methylene blue: A comparative study. *Surfaces and Interfaces*, 5, 19–29. DOI: 10.1016/j.surfin.2016.08.006.

[30] Teng, F., Zhang, G., Wang, Y., Gao, C., Chen, L., Zhang, P., Zhang, Z., Xie, E. (2014). The role of carbon in the photocatalytic reaction of carbon/TiO2 photocatalysts. *Applied Surface Science*, 320, 703–709. DOI: 10.1016/j.apsusc.2014.09.153.

[31] Li, W., Liang, R., Zhou, N.Y., Pan, Z. (2020). Carbon Black-Doped Anatase TiO2 Nanorods for Solar Light-Induced Photocatalytic Degradation of Methylene Blue. *ACS Omega*, 5(17), 10042–10051. DOI: 10.1021/acsomega.0c00504.

[32] Kavitha, R., Devi, L.G. (2014). Synergistic effect between carbon dopant in titania lattice and surface carbonaceous species for enhancing the visible light photocatalysis. *Journal of Environmental Chemical Engineering*, 2(2), 857–867. DOI: 10.1016/j.jece.2014.02.016.

[33] Sean, N.A., Leaw, W.L., Nur, H. (2019). Effect of calcination temperature on the photocatalytic activity of carbon-doped titanium dioxide revealed by photoluminescence study. *Journal of the Chinese Chemical Society*, 66(10), 1277–1283. DOI: 10.1002/jccs.201800389.

[34] He, J., Kumar, A., Khan, M., Lo, I.M.C. (2021). Critical review of photocatalytic disinfection of bacteria: from noble metals- and carbon nanomaterials-TiO2 composites to challenges of water characteristics and strategic solutions. *Science of The Total Environment*, 758, 143953. DOI: 10.1016/j.scitotenv.2020.143953.

[35] Li, Y., Li, X., Li, J., Yin, J. (2006). Photocatalytic degradation of methyl orange by TiO2-coated activated carbon and kinetic study. *Water Research*, 40(6), 1119–1126. DOI: 10.1016/j.watres.2005.12.042.

[36] Alkorbi, A.S., Muhammad Asif Javed, H., Hussain, S., Latif, S., Mahr, M.S., Mustafa, M.S., Alsaiari, R., Alhemiary, N.A. (2022). Solar light-driven photocatalytic degradation of methyl blue by carbon-doped TiO2 nanoparticles. *Optical Materials*, 127, 112259. DOI: 10.1016/j.optmat.2022.112259.